# Air-Stable Monolayer Cu₂Se Exhibits a Purely Thermal Structural Phase Transition

*Kai Qian, Lei Gao, Xiya Chen, Hang Li, Shuai Zhang, Xian-Li Zhang, Shiyu Zhu,
Jiahao Yan, Deliang Bao, Lu Cao, Jin-An Shi, Jianchen Lu, Chen Liu, Jiaou Wang,
Tian Qian, Hong Ding, Lin Gu, Wu Zhou, Yu-Yang Zhang, Xiao Lin,\* Shixuan Du,\*
Min Ouyang, Sokrates T. Pantelides, and Hong-Jun Gao\**

Materials possessing structural phase transformations exhibit a rich set of physical and chemical properties that can be used for a variety of applications. In 2D materials, structural transformations have so far been induced by strain, lasers, electron injection, electron/ion beams, thermal loss of stoichiometry, and chemical treatments or by a combination of such approaches and annealing. However, stoichiometry-preserving, purely thermal, reversible phase transitions, which are fundamental in physics and can be easily induced, have not been observed. Here, the fabrication of monolayer Cu₂Se, a new 2D material is reported, demonstrating the existence of a purely thermal structural phase transition. Scanning tunneling microscopy, scanning transmission electron microscopy, and density functional theory (DFT) identify two structural phases at 78 and 300 K. DFT calculations trace the phase-transition mechanism via the existence/absence of imaginary (unstable) phonon modes at low and high temperatures. In situ, variable-temperature low-energy electron diffraction patterns demonstrate that the phase transition occurs across the whole sample at ≈147 K. Angle-resolved photoemission spectra and DFT calculations show that a degeneracy at the $\Gamma$ point of the energy bands of the high-temperature phase is lifted in the low-temperature phase. This work opens up possibilities for studying such phase transitions in 2D materials.

The advent of monolayer graphene in 2004 as a prototype 2D material led to broad experimental and theoretical investigations of hundreds of 2D materials whose unique and unusual properties anchor novel device concepts and offer promise for applications.[1–3] Structural phase transformations of 2D materials driven by external means have been studied extensively.[4–18] For example, electron doping by alloying or intercalation and electron injection trigger phase transformations in MoS₂ and MoTe₂ monolayers.[6–9] Thermal treatment, which is the most common method to drive phase transitions in bulk materials, induces phase transformations in VS₂, VSe₂, and PtSe₂ monolayers via loss of chalcogen atoms so that reversals require fresh supplies.[10,15,18]

Stoichiometry-preserving, purely thermal, reversible structural phase transitions were studied by both experiments and theory more than 20 years ago in self-assembled monolayers of rare-gas atoms and small molecules.[19] Such monolayers are held together by weak in-plane van der Waals interactions, in contrast to bona fide 2D materials, which are held together by in-plane chemical bonds. Purely thermal phase transitions in chemically bonded 2D materials, governed by chemical-bond rearrangements, have been theoretically predicted but have not been observed in any of the 2D materials that have been investigated in the last 15 years.[20,21]

Dr. K. Qian, Dr. L. Gao, X. Y. Chen, H. Li, S. Zhang, X.-L. Zhang,
Dr. S.-Y. Zhu, Dr. J.-H. Yan, Dr. D.-L. Bao, L. Cao, J.-A. Shi, Dr. J.-C. Lu,
Prof. T. Qian, Prof. H. Ding, Prof. L. Gu, Prof. W. Zhou, Prof. Y.-Y. Zhang,
Prof. X. Lin, Prof. S.-X. Du, Prof. S. T. Pantelides, Prof. H.-J. Gao
Institute of Physics and University of Chinese Academy of Sciences
Chinese Academy of Sciences
Beijing 100190, P. R. China
E-mail: xlin@ucas.ac.cn; sxdu@iphy.ac.cn; hjgao@iphy.ac.cn
Dr. D. L. Bao, Prof. S. T. Pantelides
Department of Physics and Astronomy and Department of Electrical
Engineering and Computer Science
Vanderbilt University
Nashville, TN 37235, USA

The ORCID identification number(s) for the author(s) of this article
can be found under https://doi.org/10.1002/adma.201908314.

DOI: 10.1002/adma.201908314

Dr. J.-C. Lu
Faculty of Materials Science and Engineering
Kunming University of Science and Technology
Kunming, Yunnan 650000, China
C. Liu, Prof. J. O. Wang
Institute of High Energy Physics
Chinese Academy of Sciences
Beijing 100049, China
Prof. T. Qian, Prof. H. Ding, Prof. W. Zhou, Prof. Y.-Y. Zhang, Prof. X. Lin,
Prof. S.-X. Du, Prof. H.-J. Gao
CAS Center for Excellence in Topological Quantum Computation
Chinese Academy of Sciences
Beijing 100190, China
Prof. M. Ouyang
Department of Physics
University of Maryland
College Park, MD 20742-4111, USA

**ADVANCED
SCIENCE NEWS**
www.advancedsciencenews.com

**ADVANCED
MATERIALS**
www.advmat.de

Herein, we report a purely thermal structural phase transition in a new 2D material, monolayer $Cu_2Se$. We fabricated large-scale, high-quality epitaxial monolayer $Cu_2Se$ on bilayer graphene and observed two distinct structures at 300 and 78 K, respectively, using scanning tunneling microscopy (STM). Cross-sectional scanning transmission electron microscopy (STEM) images confirm the material's monolayer form. In situ, low-energy electron diffraction patterns were measured at a continuous temperature ranging from 78 to 300 K. We found that the phase transition occurs across the whole sample at ≈147 K. The phases below and above 147 K are named $\zeta$ and $\lambda$ phases for their zigzag and linear Cu arrangements, respectively. Density functional theory (DFT) calculations are used in conjunction with STM and STEM data to identify the structures and determine their space groups as $P2_1/c$ and $P\bar{3}m1$ for the $\zeta$ and $\lambda$ phases, respectively. DFT calculations find that the $\lambda$ phase exhibits imaginary-frequency phonons at 0 K, i.e., the phase is unstable, and the corresponding atomic displacements are precisely what is necessary to drive the system to the $\zeta$ phase. On the other hand, the $\lambda$ phase has no imaginary-frequency phonons at 300 K, i.e., it is stable. Finite-temperature quantum molecular dynamics simulations further confirm that the phase transitions are purely thermal. Angle-resolved photoemission spectroscopy (ARPES) and calculated energy bands find that a band splitting occurs at the $\Gamma$ point near the Fermi level as the $Cu_2Se$ monolayer undergoes a $\lambda$-to-$\zeta$ phase transition. The present demonstration of a purely thermal, reversible, structural phase transition in a monolayer material provides a new platform for future investigations.

The sample is prepared by direct coevaporation of Se and Cu onto bilayer graphene (BLG) (see the Supporting Information for more details). X-ray photoelectron spectroscopy (XPS) data reveal that the composition of the sample is $Cu_2Se$ (Figure S1, Supporting Information).[22] A large-scale STM image is shown in Figure S2a (Supporting Information). A zoomed-in STM image (**Figure 1**a) taken at liquid-nitrogen temperature (78 K) shows 1D stripes. An atomic-resolution STM image (Figure 1b) and its fast Fourier transform (FFT) (Figure 1c) show that the film possesses a rectangular unit cell, with a lattice constant of $a = 0.42 \pm 0.05$ nm and $b = 0.71 \pm 0.05$ nm.

Based on the STM images and previously reported predictions for bulk layered $Cu_2Se$, we constructed the atomic model shown in Figure 1d.[23,24] This $\zeta$-phase structure is the basic layer in bulk layered $Cu_2Se$ and has the space group $P2_1/c$.[23,24] The DFT-relaxed lattice constants, $a = 0.41$ nm and $b = 0.67$ nm, agree with the measured values $a = 0.42 \pm 0.05$ nm and $b = 0.71 \pm 0.05$ nm. The atomic model and corresponding simulated STM image are overlaid in Figure 1b, demonstrating that the bright spots in the STM image are top-layer Se atoms. The excellent agreement between the simulated and experimental images confirm a $\zeta$-phase $Cu_2Se$. Considering the BLG substrate, a $(1 \times 14)$ $Cu_2Se$ sitting on a $(3 \times 15\sqrt{3})$ BLG model is proposed. The 1D moiré pattern shown in Figure 1a is perfectly reproduced (Figure S3, Supporting Information).

In Figure 1e,f, we show STM images at 300 K, revealing no 1D moiré pattern. We deduced the structure of the new phase using atomic-resolution STM and STEM images (Figures 1f and **2**a, respectively) and the corresponding FFTs (Figures 1g and 2b, respectively), finding a hexagonal lattice with a higher
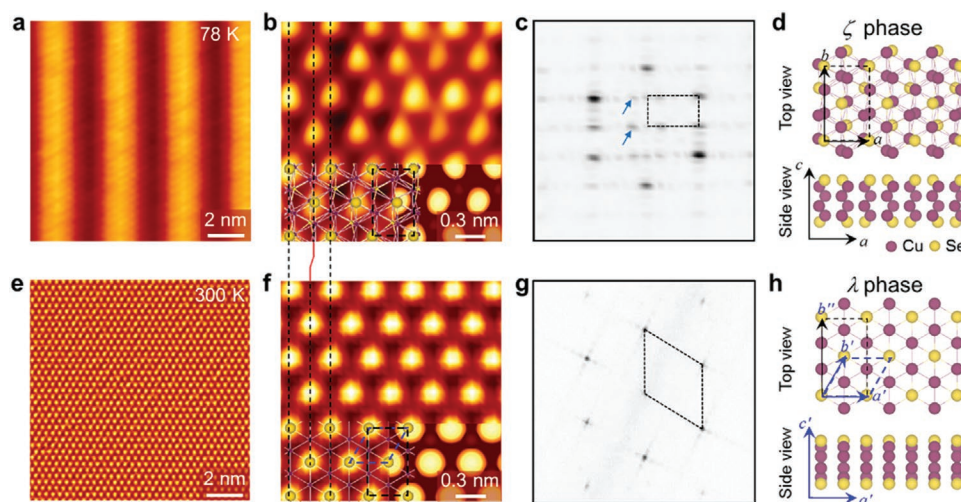


**Figure 1.** STM images and atomic configurations of monolayer $Cu_2Se$ at 78 and 300 K. a) An STM image of $Cu_2Se$ at 78 K, showing 1D moiré patterns with periodicity around 3 nm. $V_s = -1$ V, $I_t = 0.1$ nA. b) Atomic-resolution STM image of $Cu_2Se$ at 78 K. $V_s = -0.5$ V, $I_t = 0.5$ nA. An atomic model and the corresponding STM simulation are overlaid. c) FFT of (b), revealing a twofold rotational symmetry and a rectangular unit cell. The satellite spots pointed at by blue arrows correspond to the 1D moiré pattern. d) A $\zeta$-phase atomic model and the unit cell (black dashed rectangle, $a = 0.41$ nm, $b = 0.67$ nm). The Se atoms in the middle of the rectangular unit cells cause weakening of some diffraction spots in (c). e) STM image of $Cu_2Se$ at 300 K showing homogeneity. $V_s = -1$ V, $I_t = 0.1$ nA. f) Atomic-resolution STM image of $Cu_2Se$ at 300 K. $V_s = -0.5$ V, $I_t = 0.5$ nA, overlaid at the bottom with an atomic model and the corresponding STM image simulation. The dashed lines in (b) and (f) indicate the position of the STM bright spots, i.e., the position of the top-layer Se atoms, and the red polyline is used to show the displacement of some top-layer Se atoms. g) FFT of (f) showing a hexagonal unit cell. h) A $\lambda$-phase atomic model. The $\lambda$-phase has the rectangular unit cell (black dashed rectangles in (f) and (h), $a' = 0.40$ nm, $b'' = 0.69$ nm) and has a hexagonal primitive unit cell (blue dashed rhombuses in (f) and (h), $a' = b' = 0.40$ nm). Comparing with the lattice parameter of the $\zeta$-phase, the lattice parameter of the rectangular unit cell $a$ ($a'$) decreases, while $b$ ($b''$) increases. Freestanding monolayers are used for STM simulations as the interaction between $Cu_2Se$ monolayers and graphene is weak compared with the in-plane chemical bonding.

**ADVANCED
SCIENCE NEWS**

www.advancedsciencenews.com

**ADVANCED
MATERIALS**

www.advmat.de
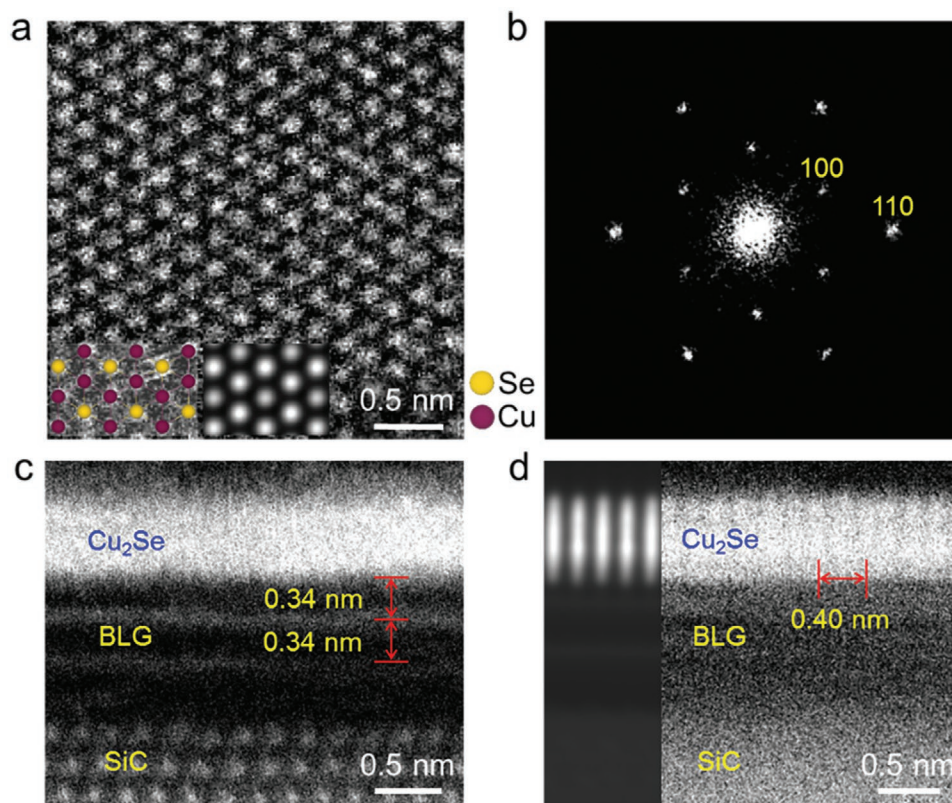
**Figure 2.** STEM images of monolayer $Cu_2Se$ at 300 K. a) Atomic-resolution plane-view image with an overlaid $\lambda$-phase atomic model and simulated image. b) FFT of (a), showing threefold rotational symmetry. c) Cross-sectional edge-on STEM image of $\lambda$-phase $Cu_2Se$ on a BLG-SiC substrate. d) Cross-sectional on-axis STEM image.

symmetry than the $\zeta$ phase. The cross-sectional STEM image in Figure 2c shows a layer thickness of $\approx 0.38$ nm, which is the same as the theoretical thickness of monolayer $Cu_2Se$ (Figure S4b, Supporting Information), confirming the sample's monolayer form. We note that the atomic columns in the cross-sectional view of Figure 2d are straight, compared with the $\zeta$-phase zigzag pattern shown in Figure 1d.

Retrieving information from the STM and STEM images, we constructed the atomic model shown in Figure 1h for the $\lambda$ phase. Comparing to the atomic arrangement in the $\zeta$ phase, the six atoms in each column are well aligned. This structure has the space group $P\bar{3}m1$. The DFT-relaxed lattice constants are $a' = b' = 0.40$ nm, in excellent agreement with the experimental values $a' = b' = 0.40 \pm 0.05$ nm. The atomic model and the corresponding simulated STM and plane-view STEM images are overlaid on Figures 1f and 2a, respectively, showing excellent agreement and thus confirming the $\lambda$-phase structure. We note that the $\lambda$ phase has never been reported either as a theoretical prediction or experimental observation.

The measured distance between monolayer $\lambda$-$Cu_2Se$ and the graphene substrate is $\approx 0.34$ nm (Figure 2c). The DFT-calculated value for this distance, 0.33 nm (Figure S4, Supporting Information), is in excellent agreement. Electron localization function (ELF) plots, shown in Figure S4 (Supporting Information), reveal weak, van der Waals interactions between the $\lambda$-$Cu_2Se$ monolayer and BLG. These interactions have minimal effect on the structure of the two phases and hence on the

phase transition, which is driven entirely by in-plane chemical-bonding rearrangements. We conclude that the phase transition is an intrinsic property of monolayer $Cu_2Se$.

In order to explore the origins of the phase transition, we compared the total energies and performed phonon calculations for both the $\lambda$ and $\zeta$ structures at $T = 0$ K. The total energy of the $\zeta$ structure is 34 meV per formula unit lower than that of the $\lambda$ structure. We found that the $\zeta$ structure has no imaginary-frequency phonon modes (Figure S5a, Supporting Information), i.e., it is stable at low temperatures, while the $\lambda$ structure has an imaginary-frequency phonon branch (Figure S5b, Supporting Information). We examined this mode's atomic displacements and found them to be precisely those that drive the linear chains into a zig-zag pattern (see Figure S5, Supporting Information). We repeated the phonon calculations at 300 K for the $\lambda$ structure and found that there are no imaginary-frequency modes, i.e., the structure is stable at room temperatures. We also ran quantum molecular dynamics simulations at 500 K using the lattice constant of the $\lambda$ structure (Figure S5d, Supporting Information), but placed the Cu atoms in zig-zag chains as in the $\zeta$-structure. The zig-zag chains quickly straighten out as in the $\lambda$ structure, fully confirming the mechanism and pathway for the observed thermal phase transition. Both structures have the same rectangular unit cell (the $\lambda$ phase has a hexagonal primitive unit cell) as shown in Figure 1d,h. During the $\zeta \rightarrow \lambda$ phase transition, the lattice parameter $a$ decreases, while $b$ increases. When
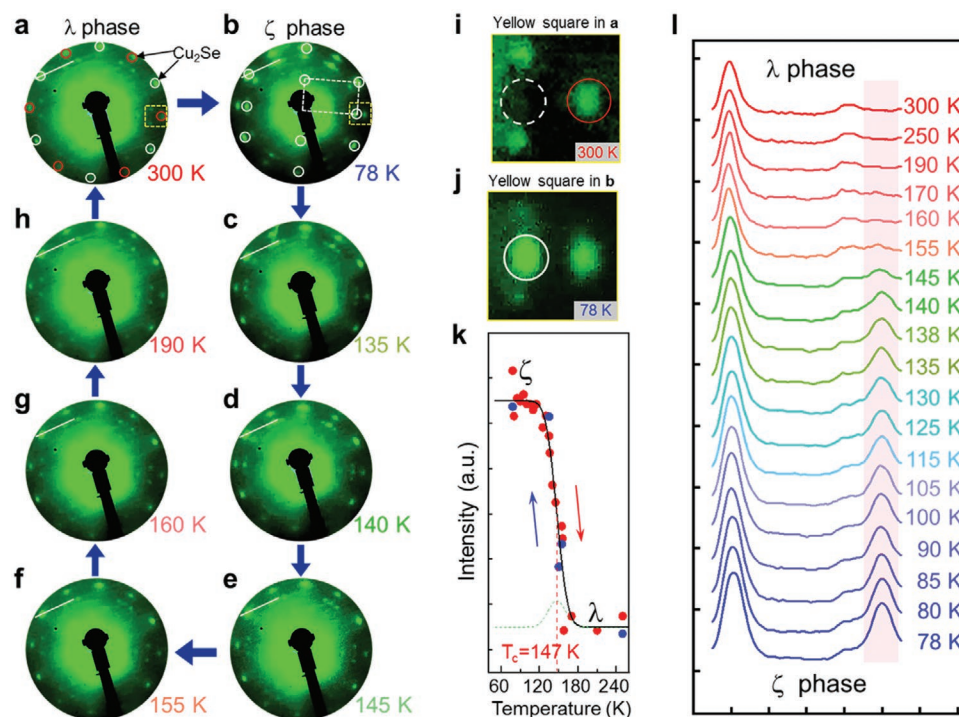
**Figure 3.** LEED patterns of monolayer $Cu_2Se$ at different temperatures. a–h) Evolution of the monolayer $Cu_2Se$ structure in $k$-space. Two sets of diffraction spots from two $\lambda$-$Cu_2Se$ domains rotated by 30° are marked by white and red solid circles while one set of diffraction spots from one $\zeta$-$Cu_2Se$ domain is marked by white dashed circles. See Figure S6 (Supporting Information) for details. i,j) Zoomed-in images from the yellow squares in (a) and (b), respectively. k) Temperature-dependent intensities of the diffraction spots indicated by white dashed circles in (j). Red and blue spots indicating the heating and cooling processes, respectively. The curve is fitted by cumulative distribution function of normal distribution. The transition temperature is ≈147 K. l) Evolution of the intensities of spots from the white line profile in LEED patterns in (a)–(h). The peaks, originating from the diffraction spots which are characteristic of the $\zeta$-phase, are highlighted by the pink window (all LEED patterns used in this figure are provided in Figure S7, Supporting Information).

$b = \sqrt{3}a$, the $\lambda$ phase is formed with higher symmetry and the primitive unit cell changes from rectangle to hexagon. On the other hand, the $\zeta$ phase structure could be considered as a distorted $\lambda$ phase structure. The displacement of some top-layer Se atoms is indicated by the red polyline connecting Figure 1b,f.

In situ, variable-temperature, LEED data shown in **Figure 3** and Figure S7 (Supporting Information) allow us to determine the phase-transition temperature. At 300 K, we see two similar sets of hexagonal diffraction spots separated by 30°, marked by white and red solid circles (Figure 3a). The two sets evolve similarly with temperature and can, therefore, be attributed as two sets of $\lambda$-phase domains (see Figure S6, Supporting Information, for details), as already inferred from STM, STEM, and DFT studies. For clarity, we monitor the evolution of only the spots marked by white circles. At $T = 78$ K, these spots evolve into a rectangular pattern marked by white dashed circles (Figure 3b), shown clearly in the zoomed-in Figure 3i,j. The emergence of new diffraction spots as shown in the white dashed circle in Figure 3j demonstrates the presence of the $\zeta$-phase structure. Raising the temperature from 78 K back to 300 K, Figure 3c–h shows that the rectangular pattern fades away and the hexagonal patterns reemerge, demonstrating that the structural phase transition is purely thermal and reversible.

The intensities of the LEED spots are plotted in Figure 3k against the sample temperature. The fitting curve reveals that

the $Cu_2Se$ $\zeta$-to-$\lambda$ phase transition is reversible and the critical temperature is around 147 K. The temperature-dependent intensity of the diffraction peaks across the white-line profile in LEED images (Figure 3a–h) is shown in Figure 3l. The peaks highlighted in pink decrease as the temperature increases, which more directly exhibits the evolution of the new spots. The fact that each phase is stable over a fairly wide temperature range above and below a transition temperature, respectively (Figure 3) indicates that there is a phase transition rather than a crossover in monolayer $Cu_2Se$.

We measured the energy band structures of monolayer $Cu_2Se$ by in situ ARPES at 78 and 300 K. **Figure 4**a,b shows the overall and second-derivative spectra for $\zeta$-phase monolayer $Cu_2Se$ at 78 K, respectively. There are three equivalent domains rotated by 120° due to the symmetry mismatch between the sample and the substrate. All domains contribute to the ARPES data. The DFT-calculated band structures along $\Gamma$–Y (black) and $\Gamma$–P/P′ (red) directions coming from different domains for the $\zeta$-$Cu_2Se$ phase are shown in Figure 4c and overlaid on Figure 4b. The agreement between the ARPES data and the calculated energy bands is excellent.

Figure 4e,f shows the ARPES results at 300 K and their second-derivative spectra, respectively. At the $\Gamma$ point near the Fermi level, the split bands at 78 K change to degenerate bands at 300 K (Figure 4e), which suggests a higher symmetry at higher temperatures. Figure 4g shows the calculated energy bands of
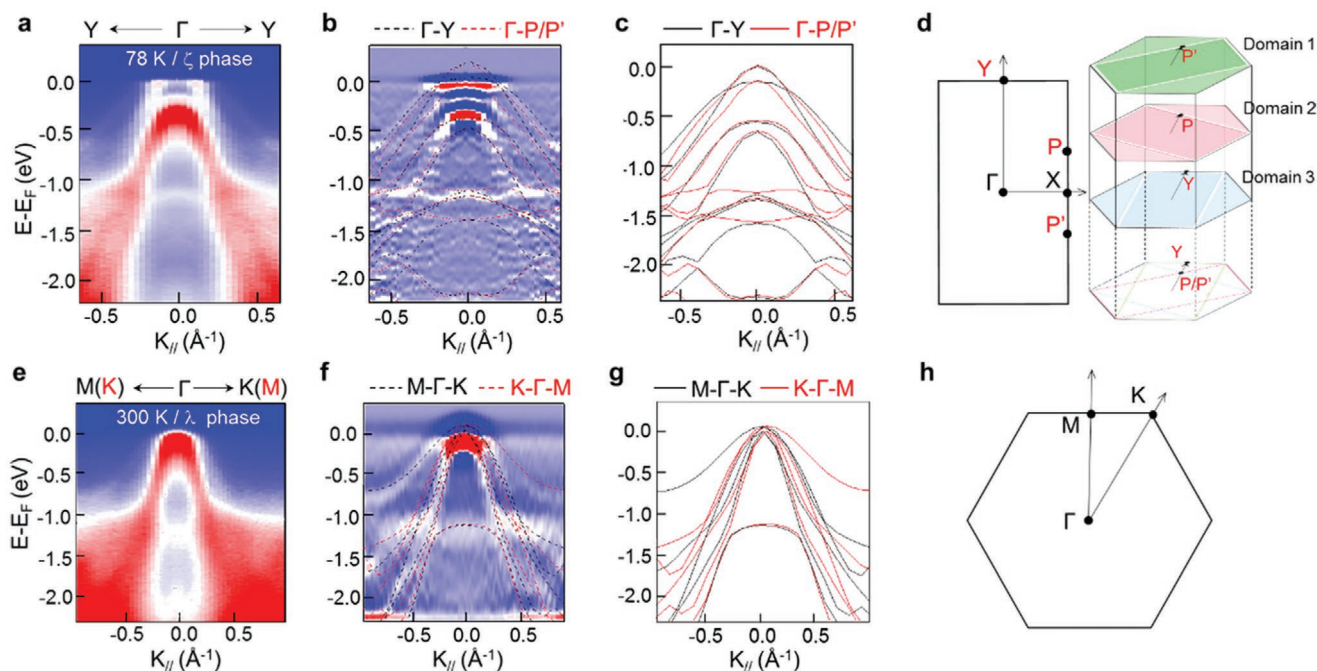
**Figure 4.** Band structures from ARPES and DFT calculations. a) Overall band structure measured along the Γ–Y direction at 78 K. b) Second-derivative spectra of (a) to enhance the low-density features. The overlaid black dashed lines are the calculated band structure along the Γ–Y direction while the red ones are along Γ–P/P′. c) Calculated band structure along the Γ–Y (black) and Γ–P/P′ (red) directions, respectively. d) Brillouin zone of ζ-Cu₂Se. Γ, Y, and P/P′ are labeled by black dots. e) Overall band structure measured along the M–Γ–K directions at 300 K. f) Second-derivative spectra of (e). The overlaid black and red dashed lines are the calculated band structures along the M–Γ–K and K–Γ–M directions, respectively. g) Calculated band structure along the M–Γ–K (black) and K–Γ–M (red) directions, respectively. h) Brillouin zone of λ-Cu₂Se (see Figure S8, Supporting Information, for details).

the $\lambda$-phase $Cu_2Se$ along the M–Γ–K (black) and the K–Γ–M (red) directions, originating from different domains. The theoretical bands are overlaid on the ARPES data in Figure 4f, showing excellent agreement. This agreement further confirms the structure of the $\lambda/\zeta$ phases and the homogeneity of the samples. In addition, the micrometer-scale homogeneity seen in Figure S2 (Supporting Information) is sufficient to allow the collection of images such as those in Figure 1. The discontinuities seen in Figure S2 (Supporting Information), however, compromise the homogeneity at the millimeter scale of LEED and ARPES, possibly giving rise to the background in the LEED images.

Calculated band structures in multiple directions of $\zeta$-$Cu_2Se$ and $\lambda$-$Cu_2Se$ are provided in Figure S9 (Supporting Information). Even though bulk $Cu_2Se$ is metallic,[25] both the $\zeta$ and $\lambda$ monolayer phases are semiconducting. $\zeta$-$Cu_2Se$ has an indirect bandgap of 1.23 eV, while $\lambda$-$Cu_2Se$ has a direct bandgap of 1.30 eV. Since both $Cu_2Se$ phases below and above the transition temperature ≈147 K are semiconductors with bandgaps larger than 1.2 eV, the observed transition is not a charge-density-wave (CDW) transition.

In conclusion, we have demonstrated a purely thermal structural phase transition in a novel monolayer material. We studied the atomic and electronic structures of monolayer $\lambda$ and $\zeta$ phases of $Cu_2Se$, and, based on temperature-dependent $k$-space structure observations, the phase transition is proved to be reversible and occurs over the entire sample. Furthermore, $Cu_2Se$ monolayers are proved to be stable in air (Figure S11a,b, Supporting Information). This purely thermal structure phase

transition in monolayer 2D material presents a potential for using monolayers in applications that exploit thermal phase transitions in bulk materials, e.g., temperature sensors.

## Supporting Information

Supporting Information is available from the Wiley Online Library or from the author.

## Conflict of interest

The authors declare no conflict of interest.

## Keywords

2D materials, epitaxial growth, phase transitions

[1] K. S. Novoselov, A. K. Geim, S. V. Morozov, D. Jiang, Y. Zhang, S. V. Dubonos, I. V. Grigorieva, A. A. Firsov, *Science* **2004**, *306*, 666.

[2] N. Mounet, M. Gibertini, P. Schwaller, D. Campi, A. Merkys, A. Marrazzo, T. Sohier, I. E. Castelli, A. Cepellotti, G. Pizzi, N. Marzari, *Nat. Nanotechnol.* **2018**, *13*, 246.

[3] K. S. Novoselov, A. Mishchenko, A. Carvalho, A. H. C. Neto, *Science* **2016**, *353*, aac9439.

[4] H. Yang, S. W. Kim, M. Chhowalla, Y. H. Lee, *Nat. Phys.* **2017**, *13*, 931.

[5] J. Wang, Y. Wei, H. Li, X. Huang, H. Zhang, *Sci. China: Chem.* **2018**, *61*, 1227.

[6] D. Rhodes, D. A. Chenet, B. E. Janicek, C. Nyby, Y. Lin, W. Jin, D. Edelberg, E. Mannebach, N. Finney, A. Antony, T. Schiros, T. Klarr, A. Mazzoni, M. Chin, Y. C. Chiu, W. Zheng, Q. R. Zhang, F. Ernst, J. I. Dadap, X. Tong, J. Ma, R. Lou, S. Wang, T. Qian, H. Ding, R. M. Osgood Jr., D. W. Paley, A. M. Lindenberg, P. Y. Huang, A. N. Pasupathy, M. Dubey, J. Hone, L. Balicas, *Nano Lett.* **2017**, *17*, 1616.

[7] S. Z. Yang, Y. Gong, P. Manchanda, Y. Y. Zhang, G. Ye, S. Chen, L. Song, S. T. Pantelides, P. M. Ajayan, M. F. Chisholm, W. Zhou, *Adv. Mater.* **2018**, *30*, 1803477.

[8] R. Kappera, D. Voiry, S. E. Yalcin, B. Branch, G. Gupta, A. D. Mohite, M. Chhowalla, *Nat. Mater.* **2014**, *13*, 1128.

[9] Y. Wang, J. Xiao, H. Y. Zhu, Y. Li, Y. Alsaid, K. Y. Fong, Y. Zhou, S. Q. Wang, W. Shi, Y. Wang, A. Zettl, E. J. Reed, X. Zhang, *Nature* **2017**, *550*, 487.

[10] F. Arnold, R.-M. Stan, S. K. Mahatha, H. E. Lund, D. Curcio, M. Dendzik, H. Bana, E. Travaglia, L. Bignardi, P. Lacovig, D. Lizzit, Z. Li, M. Bianchi, J. A. Miwa, M. Bremholm, S. Lizzit, P. Hofmann, C. E. Sanders, *2D Mater.* **2018**, *5*, 045009.

[11] J. Zhu, Z. Wang, H. Yu, N. Li, J. Zhang, J. Meng, M. Liao, J. Zhao, X. Lu, L. Du, R. Yang, D. Shi, Y. Jiang, G. Zhang, *J. Am. Chem. Soc.* **2017**, *139*, 10216.

[12] G. Eda, H. Yamaguchi, D. Voiry, T. Fujita, M. Chen, M. Chhowalla, *Nano Lett.* **2011**, *11*, 5111.

[13] D. H. Keum, S. Cho, J. H. Kim, D.-H. Choe, H.-J. Sung, M. Kan, H. Kang, J.-Y. Hwang, S. W. Kim, H. Yang, K. J. Chang, Y. H. Lee, *Nat. Phys.* **2015**, *11*, 482.

[14] D. Voiry, A. Goswami, R. Kappera, C. e Silva Cde, D. Kaplan, T. Fujita, M. Chen, T. Asefa, M. Chhowalla, *Nat. Chem.* **2015**, *7*, 45.

[15] Z. L. Liu, B. Lei, Z. L. Zhu, L. Tao, J. Qi, D. L. Bao, X. Wu, L. Huang, Y. Y. Zhang, X. Lin, Y. L. Wang, S. X. Du, S. T. Pantelides, H. J. Gao, *Nano Lett.* **2019**, *19*, 4897.

[16] S. Cho, S. Kim, J. H. Kim, J. Zhao, J. Seok, D. H. Keum, J. Baik, D.-H. Choe, K. J. Chang, K. Suenaga, S. W. Kim, Y. H. Lee, H. Yang, *Science* **2015**, *349*, 625.

[17] Y. C. Lin, D. O. Dumcencon, Y. S. Huang, K. Suenaga, *Nat. Nanotechnol.* **2014**, *9*, 391.

[18] X. Lin, J. C. Lu, Y. Shao, Y. Y. Zhang, X. Wu, J. B. Pan, L. Gao, S. Y. Zhu, K. Qian, Y. F. Zhang, D. L. Bao, L. F. Li, Y. Q. Wang, Z. L. Liu, J. T. Sun, T. Lei, C. Liu, J. O. Wang, K. Ibrahim, D. N. Leonard, W. Zhou, H. M. Guo, Y. L. Wang, S. X. Du, S. T. Pantelides, H. J. Gao, *Nat. Mater.* **2017**, *16*, 717.

[19] L. W. Bruch, R. D. Diehl, J. A. Venables, *Rev. Mod. Phys.* **2007**, *79*, 1381.

[20] R. X. Fei, W. Kang, L. Yang, *Phys. Rev. Lett.* **2016**, *117*, 097601.

[21] J. Liu, S. T. Pantelides, *Appl. Phys. Express* **2018**, *11*, 101301.

[22] S. C. Riha, D. C. Johnson, A. L. Prieto, *J. Am. Chem. Soc.* **2011**, *133*, 1383.

[23] M. C. Nguyen, J. H. Choi, X. Zhao, C. Z. Wang, Z. Zhang, K. M. Ho, *Phys. Rev. Lett.* **2013**, *111*, 165502.

[24] H. Chi, H. Kim, J. C. Thomas, G. Shi, K. Sun, M. Abeykoon, E. S. Bozin, X. Shi, Q. Li, X. Shi, E. Kioupakis, A. Van der Ven, M. Kaviany, C. Uher, *Phys. Rev. B* **2014**, *89*, 195209.

[25] D. Byeon, R. Sobota, K. Delime-Codrin, S. Choi, K. Hirata, M. Adachi, M. Kiyama, T. Matsuura, Y. Yamamoto, M. Matsunami, T. Takeuchi, *Nat. Commun.* **2019**, *10*, 72.